Progress In Electromagnetics Research M, Vol. 44, 191–201, 2015

Radiated Near-Field Emission Extraction on 3D Curvilinear Surfaces from 2D Data

Blaise Ravelo*

Abstract—This paper deals with a fast and simple computational method of 3D near-field (NF) radiation from 2D planar frequency- and time-dependent data. The established calculation method can be used to predict the electromagnetic (EM) emission from various types of electronic devices. The proposed method is originally applicable to the computation of the EM NF along the arbitrary shaped curvilinear 3D surface of multi-shape objects. The EM computation consists in the application of the planar NF-to-NF transform using plane wave spectrum. The relevance of the established method is verified with three different validation tests of analytical and practical demonstrations. The first validation is based on the analytical NF radiation from set of elementary dipoles excited by a harmonic signal. The second validation test is based on the experimented data from a hybrid active printed circuit boards (PCBs) in the frequency domain. The last validation test is performed with the measured NF data from a microstrip planar circuit in the time-domain. For all the different test cases, the plots of EM NF on arbitrary curvilinear surfaces are presented. Applications with 3D visualization or holographic surface with arbitrary geometry of EM radiation from planar data in both frequency- and time-domains confirm the effectiveness of the proposed method to predict the EM NF emission from complex PCBs. The developed 2D-to-3D computational method is particularly useful for radiated EM compatibility engineering.

1. INTRODUCTION

With the increase of electronic design complexity and operating frequency, electromagnetic (EM) radiation becomes harmful between the neighboring circuits [1, 2]. The EM field interactions with the neighboring electronic printed circuit boards (PCBs) become more and more crucial for the embedded systems [3]. Several EM measurement techniques are suggested to predict the planar EM emission from complex electronic circuits in the near- [4–6] and far-zone [7, 8] of the culprit sources. But, most of the developed radiating EM compatibility (EMC) techniques are costly and generally based on the far-field radiation pattern measurements which are particularly dedicated to the antenna applications [7–9]. Different from the near-field (NF) investigation, numerous regulation international standards as IEC/EN55022 [10] and IEC/EN61000-4-3 [11] are currently available with respect to the EMC conformity of electronic equipment against the emission and immunity radiations. Therefore, further investigations are still needed notably during the design and manufacturing cycle of electronic components and systems. The main bottlenecks encountered by the electronic designers can be reformulated to the EM field emission level and the radiation source location. A determination method of incoherent EM radiation source reconstruction method established from the experimental process was proposed [12]. A NF imaging technique offering the possibility to visualize and extract the common-mode currents from near transmission line discontinuities was presented in [13]. To realize a

Received 12 June 2015, Accepted 10 September 2015, Scheduled 8 December 2015

* Corresponding author: Blaise Ravelo (blaise.ravelo@esigelec.fr).

The author is with the IRSEEM EA 4353, Graduate School of Engineering ESIGELEC, Technopôle du Madrillet, Avenue Galilée, F-76801 Saint Etienne du Rouvray, France.

high resolution 2D measured fields, those techniques require an electromechanical automated test bench as developed in [5, 6, 14, 15] for the EM NF scanning in a planar surface located in the proximity of the radiating devices. Nevertheless, those techniques are still limited to the regular shape of scanning surface. The existing techniques are notably valid in function of the targeted 3D zones of interest in the proximity of the device under test in addition the measurement accuracy and the operating radio frequency (RF) bands [16].

To overcome these technical limits, behavioral models of EM NF based on the equivalent elementary EM dipole array were suggested [15, 17]. One of the most popular EM NF emission model is based on the inverse method whose parameters are extracted from the planar measured data. However, on the one hand, the popular full wave simulation tools as CST [18], EMPro [19], HFSS [20], EMCoS [21] and FEKO [22] which are especially dedicated to the EM computations are not appropriate to the PCBs with typically complex structures and containing several integrated circuits. On the other hand, the EM NF scanning techniques [5, 6, 14–16] are still very expensive and time consuming. Furthermore, the associated NF radiation processing methods are hardly practical for predicting EM emission in the 3D zones located nearby the radiating devices [23]. Different from the EM far-field radiation analyses, the evanescent and non-uniform waves are of crucial importance when the NF emission interacts with a sensitive electronic circuit [1, 2, 16].

To face this difficulty, NF-to-NF extraction and post-processing methods were proposed [4, 24–26]. However, the approach introduced in [4] is established from the frequency domain far-field data applied to the analytical processing the multipole identification of spherical Hankel function. The method is not accurate enough for the EM plots under millimeter resolutions, and it is strictly limited to the spherical representation particularly. Moreover, other EM computation methods from near-field 2D data much more adapted to the far-field pattern are proposed in [24]. But such a method is particularly time consuming and cannot predict the EM field in the arbitrary zone close to the culprit radiating devices. By using the plane wave spectrum (PWS) transform, fast and accurate EM computational methods for the NF processing are developed in [25, 26]. So far, the PWS theory was only used for the planar EM NF treatment and to predict the field cartographies. The transposition of the NF-NF transform in the time domain for the radiated EMC analysis is addressed in [26].

Despite the existing NF processing methods available in the literature, the prediction of NF levels on the 3D surface of multi-shape objects from complex electronic systems as PCBs has never been done. For this reason, in this paper, a fast and easy computational method is established and applied to the experimental NF data to plot the EM NF on 3D arbitrary surfaces. The proposed method is originally flexible for predicting 3D EM emission from radiating devices with the possibility of fast transient perturbations consideration. After the methodology description, numerical investigations showing relevant predictions of EM radiation emitted by different types electronic PCBs in both frequency- and time-domains will be investigated.

2. METHODOLOGY OF THE PROPOSED NF PROCESSING FOR THE 3D PLOTTING

This section is fundamentally focused on the description of the computational method principle. The routine algorithm mechanism of the NF processing method under study will be highlighted. The analytical formulations illustrating the mathematical operation on the 2D data treatment are established. Then, different steps of the computational method taking into account the 3D plotting on surfaces presenting arbitrarily geometry exposed to the EM-NF from the radiating devices are described.

2.1. Mathematical Approach

For the analytical approach, the EM (electrical and magnetic denoted respectively E and H) field data are mathematically represented by $\overrightarrow{X}(x, y, z_{\min})$. This 2D initial data are defined in the horizontal plane situated at the height $z_{\min}$ delimited by $x_{\min}$, $x_{\max}$, $y_{\min}$ and $y_{\max}$ in the $(Oxyz)$ system reference. Then, one is represented by $\overrightarrow{X}(x, y, z, f)$ the EM (E- or H-) fields defined in the rectangular coordinate $(Oxyz)$ at the operating frequency f. By assuming the wave vector defined as $\vec{k} = k_x\vec{u}_x + k_y\vec{u}_y + k_z\vec{u}_z$

that the radiating source plane is in parallel with (Oxy)-plane, the discrete formulation of the field $\overrightarrow{X}$ plane wave spectrum (PWS) is defined as:

$$\overrightarrow{P}_X = \frac{\Delta x \cdot \Delta y}{2\pi} \sum_{m=1}^{m_{\max}} \sum_{n=1}^{n_{\max}} \overrightarrow{X} e^{j(k_x x_m + k_y y_n)}. \tag{1}$$

Similar to the 2D fast Fourier transform (FFT), the associated inverse PWS (IPWS) is written as:

$$\overrightarrow{X} = \frac{\Delta k_x \cdot \Delta k_y}{2\pi} \sum_{m=1}^{m_{\max}} \sum_{n=1}^{n_{\max}} \overrightarrow{P}_X e^{-j(x \cdot k_{x_m} + y \cdot k_{y_n})}. \tag{2}$$

The discretization of $\overrightarrow{X}(f)$ for example with the planar representation in $(Oxyz)$ requires the geometrical parameters delimited by ($x_{\min}$, $x_{\max}$, $y_{\min}$, $y_{\max}$,) and the associated space steps defined by (Δx, Δy, Δz) as depicted in Fig. 1. In order to perform the NF processing with the PWS computation, the data should be represented in the dual space frequency area. By this way, the space-frequency discrete parameters were determined. First, the x- and y-frequency space parameters are also linked to the wave vector components given by:

$$\begin{cases} k_{\xi\,\max} = -k_{\xi\,\min} = \dfrac{\pi}{\Delta\xi} \\ \Delta k_\xi = \dfrac{2\pi}{\xi_{\max} - \xi_{\min}} \end{cases}, \tag{3}$$

with $\xi = (x, y)$. In this case, z-component of the wave vector is expressed as:

$$k_z = \begin{cases} \sqrt{k^2 - k_x^2 - k_y^2} & \text{if} \quad k^2 \geq k_x^2 + k_y^2 \\ -j\sqrt{k_x^2 + k_y^2 - k^2} & elsewhere \end{cases}, \tag{4}$$

with j the imaginary complex number and $k = \frac{2\pi f}{v}$ (the wave number) by denoting v the wave speed.

The first case of this equation describes the propagating waves, and then the other one is the evanescent waves. In the PWS space, the wave vector respects the translation property for example along the z-direction:

$$\overrightarrow{P}_X(z = z_2) = \overrightarrow{P}_X(z = z_1) \cdot e^{-jk_z \cdot (z_2 - z_1)}. \tag{5}$$

By combining expression (5) with Equations (1) and (2), the transformation of $\overrightarrow{X}(z = z_1)$ into $\overrightarrow{X}(z = z_2)$ can be realized. It is noteworthy that this PWS translation transformation operates only with $z_2 > z_1$. The generalized methodology allows the generation of NF-to-NF transformation with PWS method. Fig. 2 illustrates the configuration of the parallelepiped 3D zone of interest which is delimited by $z_{\min}$ and $z_{\max}$.

2.2. Methodology

In the present paper, during the computation, the metallic surface plane of the planar device under test (DUT) is supposed as the reference $z = 0$. The numerical implementation of the NF processing established method requires the discretization of the EM data and also the 3D space under consideration. The computational method principles can be projected into routine algorithm consisting of the following steps:

- Step 1 is the geometrical parameters definition of the input and initial 3D data as represented in Fig. 1. Then, the 3D zone of interest needs to be determined. Then, the EM field levels in the surface definition are computed.
- Step 2 consists in the extraction of the EM NF $\overrightarrow{X}(x, y, z_{test}) = f(\overrightarrow{X}(x, y, z_{\min}))$ in the test plane $z = z_{test}$ localized in a 3D near-zone above the radiating devices. In this step, the NF-NF transform introduced in [4] is applied.
- Step 3 is the calculation of the EM field vertical component X_z from only X_x and X_y based on the relation $X_z = f(X_x, X_y)$. This expression is realized with the PWS theory combined with the property of orthogonality.

- In Step 4, the 3D view is the reconstruction of the NF radiation based on the observation curvilinear surfaces $z_s = f(x_s, y_s)$ of interest (Fig. 1) with the following approximation

$$X_\xi(\min|x_s - x_m|, \min|y_s - y_n|, \min|z_s - z_p|)|_{\substack{m=1,m_{\max}\\ n=1,n_{\max}\\ p=1,p_{\max}}} . \quad (6)$$

- For the case of time-domain, a supplementary step of FFT/IFFT and convolution with the excitation perturbations is needed as Step 5. The determination of $|X(t,z{=}z_{test})|$ adapted to the 3D object of interest geometry is carried out based on the combination of NF-NF and time-frequency transforms as described in [9].

It is worth noting that the root mean squares (RMSs) of error vector magnitude (EVM) between the computed fields from the NF-NF processing and the reference are generated with the following formula:

$$\varepsilon_\xi = \frac{\sqrt{\sum_{(m,n)=(1,1)}^{(m,n)=(m_{\max},n_{\max})} |X_{\xi m}(x_m, y_n) - X_\xi(x_m, y_n)|^2}}{\sqrt{\sum_{(m,n)=(1,1)}^{(m,n)=(m_{\max},n_{\max})} |X_\xi(x_m, y_n)|^2}}, \quad (7)$$

where $\xi{=}\{x$ or y or $z\}$.

In the remainder of this paper, applications of the PWS method under study for frequency- and time-domain EM emissions from various types of radiating devices will be explored. The results to be presented in the next sections were obtained with the routine algorithm run with Matlab.

3. VALIDATION OF THE NF-NF METHOD WITH ANALYTICAL AND NUMERICAL COMPUTATIONS WITH ELEMENTARY DIPOLE RADIATION

The EM NF radiations presented in this section are computed from a set of four elementary electric dipoles placed in the horizontal plane defined by $z = 0$. The (x,y)-coordinates of each dipole center are $\{(0, 0), (7\,\text{mm}, 0), (-4\,\text{mm}, 4\,\text{mm}), (-4\,\text{mm}, -4\,\text{mm})\}$. Each dipole is ideally excited with harmonic signal having amplitude $1\,\text{mA}\cdot\text{m}$ and operating at the frequency 1 GHz.

As input data of the NF-NF processing, the planar E-field components shown in Fig. 3 were calculated based on the elementary dipole radiation formulations as defined in [27]. The NF maps are visualized in the plane $z = z_{\min} = 4\,\text{mm}$ delimited by $x_{\max} = -x_{\min} = 3\,\text{cm}$ and $y_{\max} = -y_{\min} = 4\,\text{cm}$

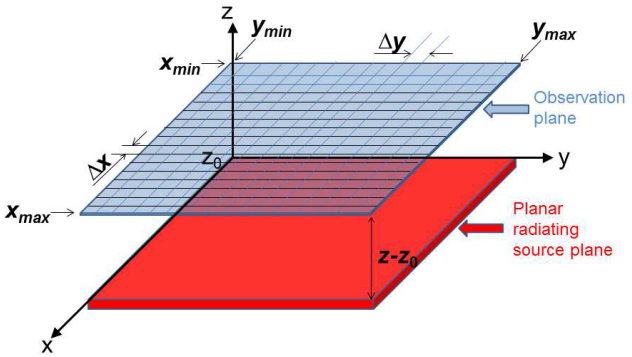

Figure 1. Geometrical configuration and parameters of the initial 2D scanned data.

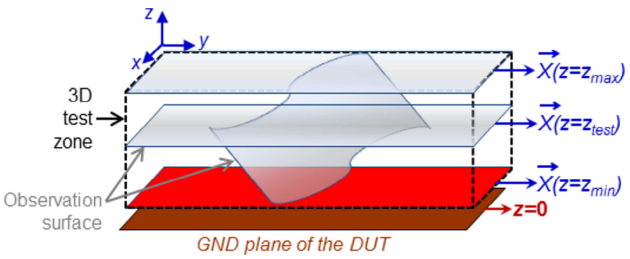

Figure 2. Illustration of the proposed NF visualization on a 3D virtual surface in the proximity of the radiating electronic PCB.

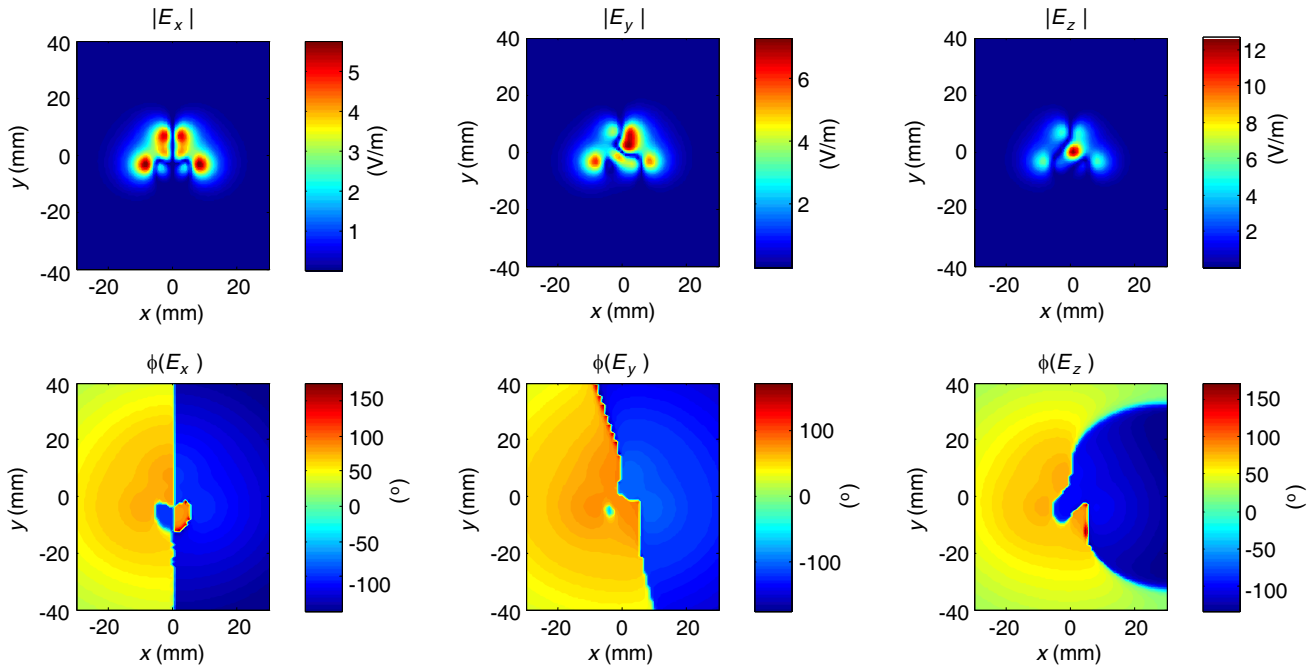

Figure 3. Initial 2D data: E-NF components at $z = 5\,\text{mm}$ and $f = 1\,\text{GHz}$.

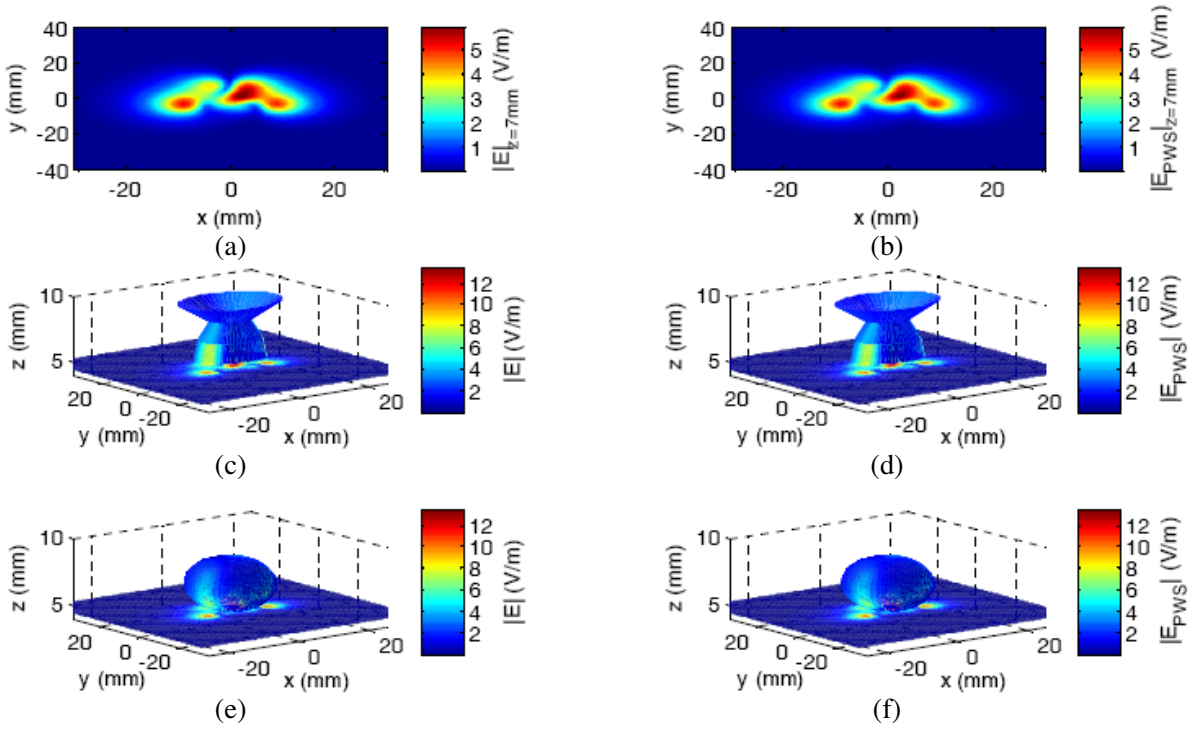

Figure 4. Comparison of 3D E-NF radiations from the direct calculation and the PWS method.

step $\Delta x = \Delta y = 1\,\text{mm}$. E-NF emission comparisons from the PWS method and direct analytical calculation at $z = 7\,\text{mm}$ are displayed in Figs. 4(a) and 4(b). A good agreement between the behaviours of E-field cartographies in the plane placed at $z = 7\,\text{mm}$ can be found. As the truncated edge effect is negligible, the same computations can be performed to any horizontal surfaces in the near zone of the radiating dipole element planes. The successive computation with vertical step Δz which can be defined

in function of the required accuracy to determine the E-NF in the parallelepiped with height $z_{\max} - z$. Then, the 2D-to-3D transform is performed via the intersection of any curvilinear surface (presenting arbitrary shape) with the gridded rectangular volume. Consequently, the operation generates a 3D plot of the NF radiation. As application example, the E-fields radiated on the 3D cylinder (Figs. 4(c) and 4(d)) and ellipsoid (Figs. 4(e) and 4(f)) curvilinear surfaces localized in the proximity zone delimited by $z_{\max} = 10\,\text{mm}$ are well correlated. The CPU time to generate the presented results was about 10 ms for the vertical space step Δz= 0.5 mm. The EVM relative was less than 2%.

Despite the efficiency of the computational method to reproduce the EM NF radiation, the result accuracies can not be guaranteed when the initial data at the edge of the considered observation surface ($x = \{x_{\min}$ or $x_{\max}\}$and $y = \{y_{\min}$ or $y_{\max}\}$) are not close to zero. It means that the extrapolation of the method to the EM far-field prediction remains quite difficult.

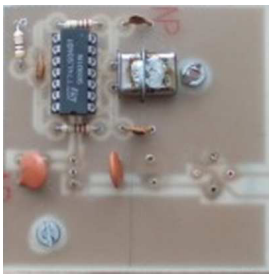

(a)

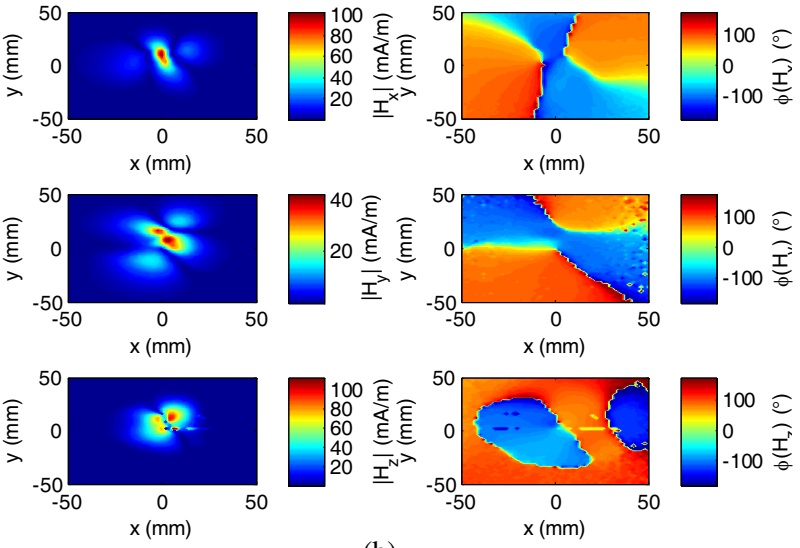

(b)

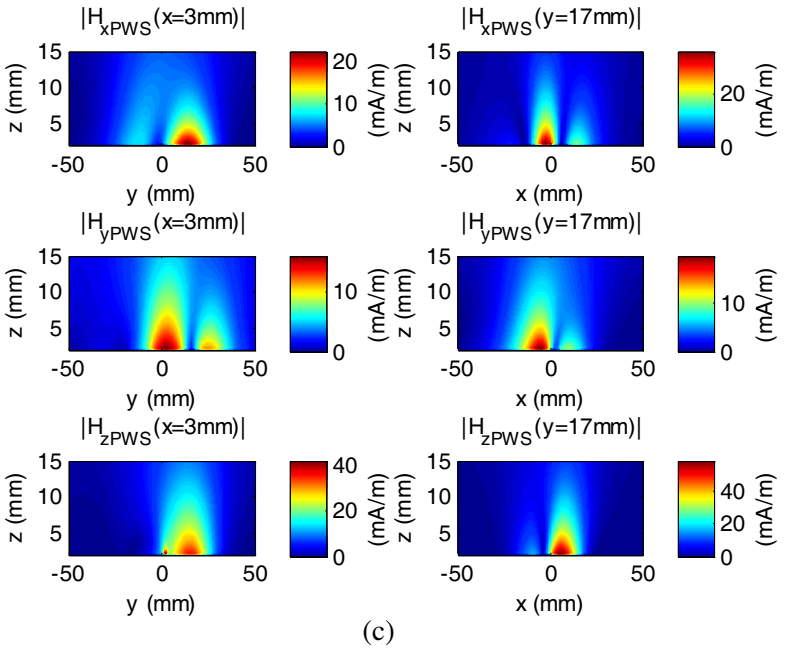

(c)

Figure 5. (a) Radiating active circuit under study. (b) Initial 2D data: measured H-NF at $z = 2\,\text{mm}$ and $f = 40\,\text{MHz}$. (c) Vertical surface mapping of H-NF extracted from the initial data.

4. EXPERIMENTAL ANALYSES WITH ACTIVE PCB NF EMISSION IN THE FREQUENCY DOMAIN

As input data of the computation results presented in this section, the measured and scanned H-NF horizontal components H_x, H_y and H_z radiated by the PCB shown in Fig. 5(a) are considered. This planar active circuit was printed on an FR4 epoxy substrate having 35 µm-thickness etched with metallic copper.

Due to the design complexity with the integrated circuit, the active circuit cannot be simulated with the commercial tools using full wave simulation to predict the 3D EM NF emission. This justifies why a more reliable computation method for the EM NF radiation analysis is introduced in this paper. It allows the determining of the radiation in this zone of interest by calculating of the overall EM-NF levels. The H-NF magnitude and phase maps of the initial 2D data at 40 MHz which serves for the 3D computation are visualized in Fig. 5(b). Those maps were realized with the NF scanning technique by using a metallic dipole loop as reported in [15, 16].

The observation scanning surfaces are defined in the horizontal plane placed $z_{\min} = 2$ mm defined in the discrete rectangular surface $x_{\max} = -x_{\min} = y_{\max} = -y_{\min} = 5$ mm step $\Delta x = \Delta y = 2$ mm. The NF measurement and calibration were performed at the IRSEEM laboratory under the condition tests as described in [15, 16]. After the application of PWS computation, the H-NF maps in the arbitrary chosen vertical surfaces along x- and y-axes presented in Fig. 5(c) were extracted. These results illustrate the feasibility of the computation method by considering the field level in function of the distance with radiation source.

As expected, the EM NF level is inversely proportional to the distance between the observation point and the radiating PCBs. Furthermore, the NF-NF transformation allows the accurate analysis of the EM radiations in various configurations of combined vertical planes. The x-, y- and z-components of the H-fields present a relative variation about {20%, 10% and 10%} for z varied from 2 mm to 15 mm respectively in the arbitrarily chosen test vertical surface plane $x = 3$ mm. A similar effect can be noticed for the perpendicular test vertical surface plane $y = 17$ mm. By assuming the computation space as a vacuum and any arbitrary vertical planes situated in the near zone delimited by $z > 2$ mm, the level of the radiated NF H-field can be computed by the same process. Therefore, the H-NF grid data can be generated in the rectangular parallelepiped defined by the 3D meshes Δx, Δy and Δz. Then, the 3D curvilinear plot can be extracted by the intersection of the 3D coordinates of the considered surface in the area of the rectangular parallelepiped. The space precision can be improved by using the Matlab interpolation functions as "*griddatan*" and "*interpn*".

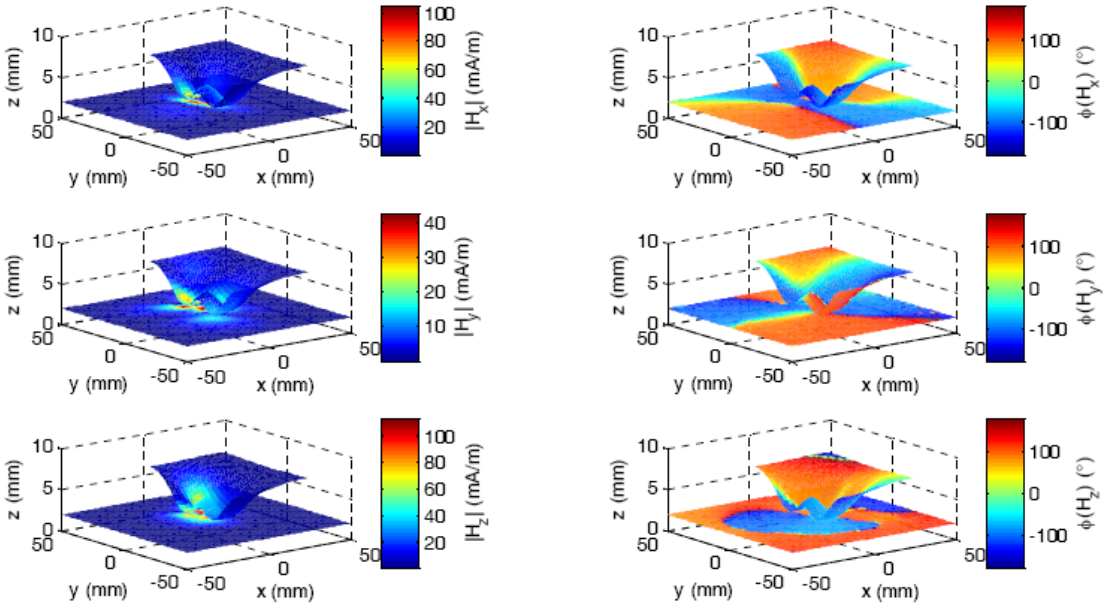

Figure 6. 3D plots of H-NF magnitude and phase on curvilinear surface.

An illustrative example of the computed 3D view of the H-NF magnitudes and phases on the arbitrary shape objects as a truncated Mexican hat is depicted in Fig. 6. It is worth noting that the H-field amplitude is higher in the minimum valley of the considered 3D surface. However, the phase behavior does not depend on the distance with the reference plane of the radiating PCB. The zone of phase transition can be found independently for the height z. It should be emphasized that the CPU time of the whole PWS routine implemented in Matlab was about 0.3 s on a Windows 7 PC with Intel® Core™ i3-3120M processor and 8Gbytes of RAM.

As expected, we can observe that the EM radiation levels are decreased when height z is increased. These computation results highlight how the EM NF radiations vary on the surface of the multi-shape object.

5. APPLICATIONS OF THE NF-NF METHOD WITH PASSIVE MICROSTRIP CIRCUIT NF EMISSION IN THE TIME-DOMAIN

In this section, the application of the 2D-to-3D NF computational method under study into time-domain applications is investigated. To do this, the magnetic NF emitted by the PCB photographed in Fig. 7(a) is investigated in this section. This microstrip circuit was printed on an FR4 substrate etched with 35 µm thickness copper. The considered excitation pulse having 1 A amplitude, 10 ns time duration and 1 GHz modulating frequency is plotted in Fig. 7(b).

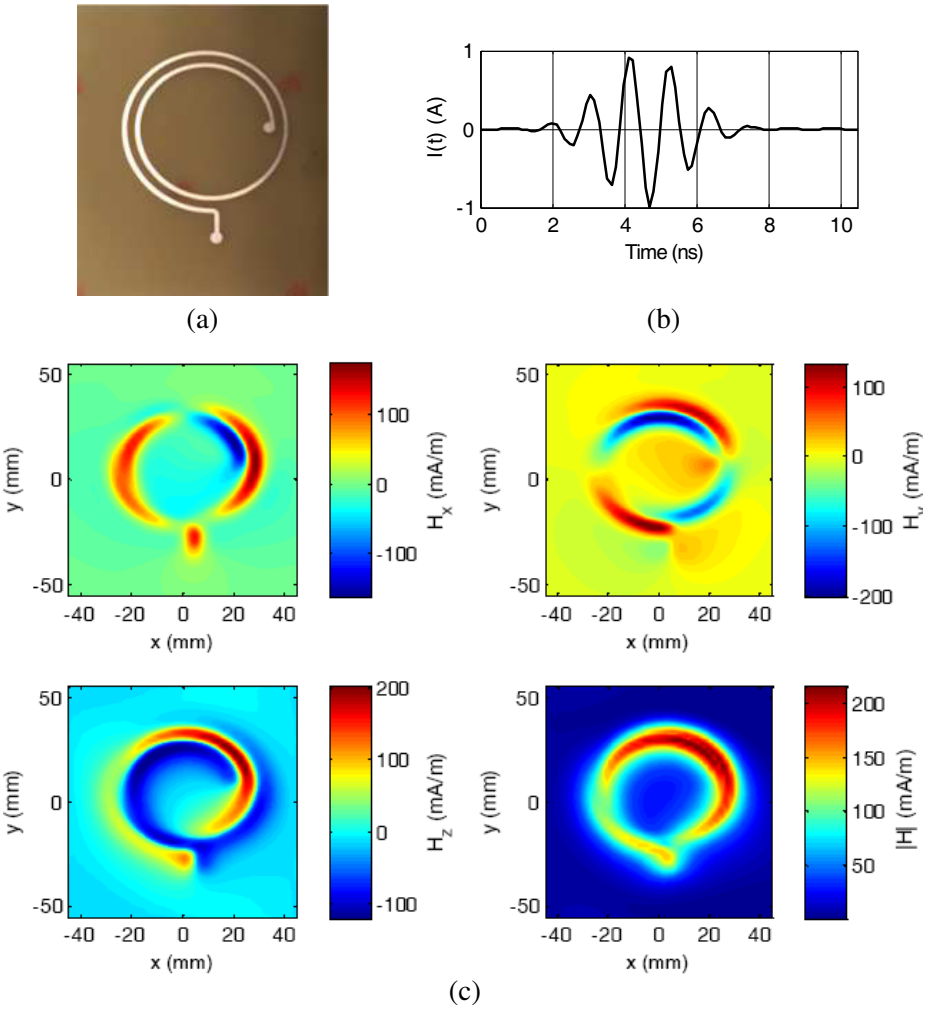

Figure 7. (a) Microstrip passive circuit under test and (b) the considered excitation signal. (c) Initial 2D data: H-NF component maps at $z = 5$ mm and $t = 5$ ns.

The initial 2D data $H_{x,y,z}(t = 5\,\text{ns})$ and $|H(t = 5\,\text{ns})|$ representing the H-NF radiation from the DUT shown in Fig. 7(a) are depicted in Fig. 7(c). The observation plane surface was positioned at $z_{\min} = 5\,\text{mm}$ and delimited by $x_{\max} = -x_{\min} = 45\,\text{mm}$ and $y_{\max} = -y_{\min} = 55\,\text{mm}$ step $\Delta x = \Delta y = 2\,\text{mm}$. During the computation, the sampling period was 0.2 ns. It is noteworthy that the presented time-domain data were extracted from the 2D data measured in the frequency domain as proposed in [26].

Similar to the previous section, after extraction of $|H(t)|$ from $H_x(t)$ and $H_y(t)$, the NF data along 3D curvilinear surfaces can be determined based on the PWS method introduced in Fig. 2. The present computation should be performed with respect to the Nyquist-Shannon sampling theorem in

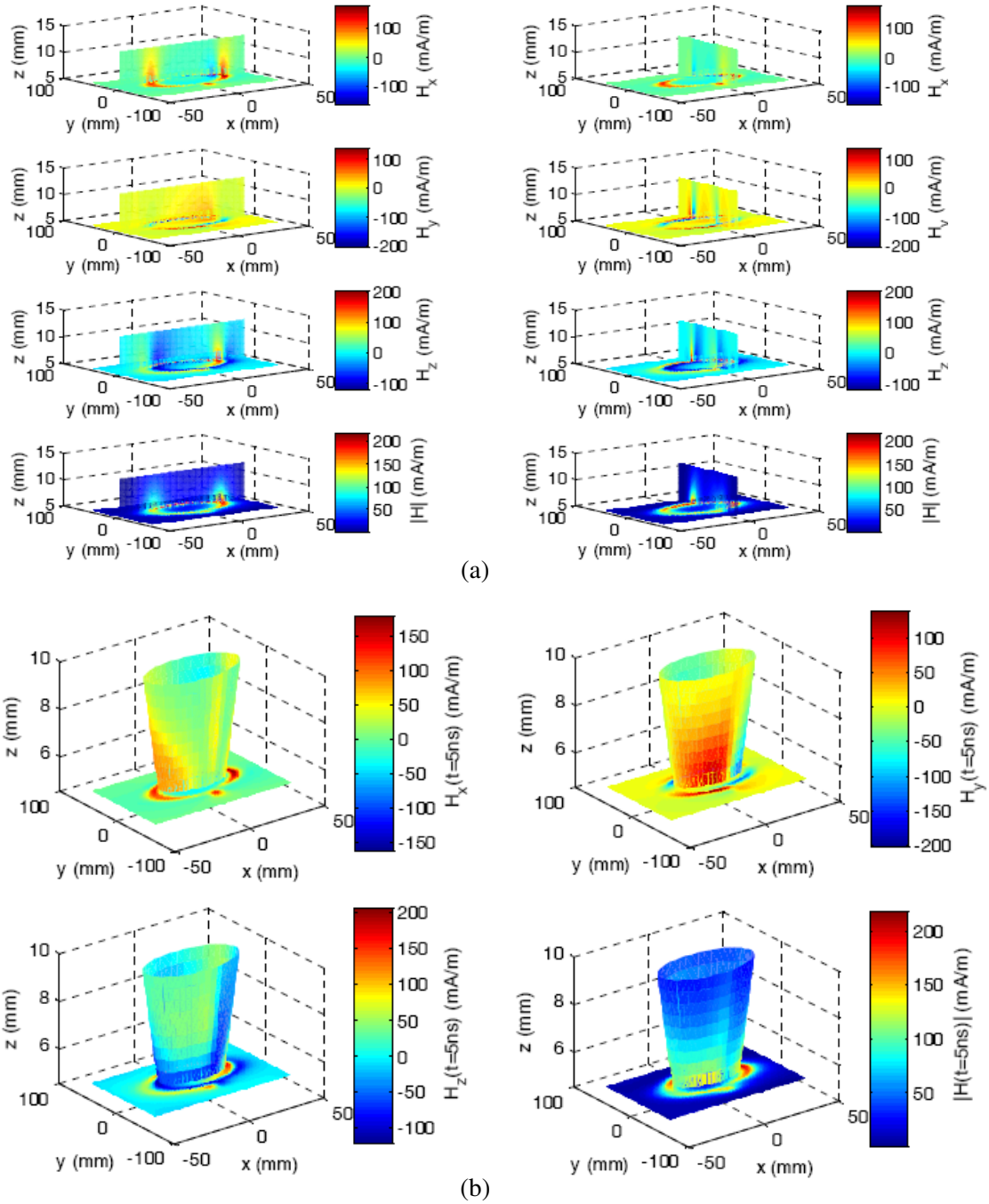

Figure 8. (a) Computed H-NF at $t = 5\,\text{ns}$ in the vertical surfaces along x- and y-axes. (b) Computed 3D NF radiation on cylindrical object at $t = 5\,\text{ns}$.

time- and space-domains for both PWS and FFT operations. The successive PWS transform associated with FFT/IFFT operations can generate 3D gridded data in the parallelepiped delimited by the lower surface $z = 5\,\mathrm{m}$ from $t_{\min}$ to $t_{\max}$. The intersection of any 3D curvilinear surface with the inner points of the parallelepiped permits the reconstruction of the time-dependent H-NF data. Application examples of the computed NF radiation along the vertical surfaces are mapped in Fig. 8(a). Once again, the decrease of the H-NF amplitude as predicted by Green function is realized with these computed data. These results indicate the overview of zones where the circuit under study radiation can be critical. With the various view, the space-time location of the critical zones can be visualized easily. The H-field component 3D plots along arbitrary shaped object as tapered cylinder are shown in Fig. 8(b).

For these last application results, the CPU time of the NF-NF computation was 4.2 seconds by considering the space resolution $\Delta z = 0.2\,\mathrm{mm}$.

6. CONCLUSION

A simple and fast EM computational method of NF emission from 2D-to-3D with arbitrary shape surface is investigated. The NF processing method is based on the PWS NF-NF transform, which can be used to analyze the EM radiation on 3D objects placed near the culprit radiating electronic components or PCBs from the initial 2D NF data. The proposed method was verified efficiently with EM NF radiation from analytical sources and PCBs in both frequency- and time-domains. The NF-NF method offers advantages in terms of simplicity, accuracy and CPU time speed. Moreover, the method can be potentially used to investigate, with easy way, the EM NF radiation from complex devices as the PCB presented earlier in Fig. 5(a) knowing only the X_x and X_y horizontal field components.

However, the drawbacks of the proposed 2D-to-3D computational method are:

- The sensitivity of the PWS transform on the computed data in function of the initial data inaccuracies.
- The truncated effects if the EM field values are not negligible at the edge ($x = \{x_{\min}$ or $x_{\max}\}$ and $y = \{y_{\min}$ or $y_{\max}\}$) of the initial observation surface.
- Difficulties to extrapolate the method to the EM far-field computation.
- Time- and space-frequencies constraints with respect to the Nyquist–Shannon sampling theorem.

Research work on the investigated NF-NF method applications for the radiated EMC measurements and post-processing of embedded electronic equipment is in progress.

ACKNOWLEDGMENT

Acknowledgement is made to the Upper Normandy Region for the PULSAT project support of this research work through the FEDER funding.

REFERENCES

1. Lertsirimit, C., D. R. Jackson, and D. R. Wilton, "Time domain coupling to a device on a printed circuit board inside a cavity," *Radio Science*, Vol. 40, No. 6, 1–12, RS6S14, Dec. 2005.
2. Archambeault, R., C. Brench, and S. Connor, "Review of printed-circuit-board level EMI/EMC issues and Ttools," *IEEE Trans. EMC*, Vol. 52, No. 2, 455–461, 2010.
3. Barrière, P. A., J. J. Laurin, and Y. Goussard, "Mapping of equivalent currents on high-speed digital printed circuit boards based on near-field measurements," *IEEE Tran. EMC*, Vol. 51, No. 3, 649–658, Aug. 2009.
4. Klinkenbusch, L., "Time domain near-field to near-field transformation using a spherical multipole approach," *Radio Science*, Vol. 46, No. 5, 1–8, RS0E17, Oct. 2011.
5. Weng, H., D. G. Beetner and R. E. DuBroff, "Prediction of radiated emissions using near-field measurements," *IEEE Trans. EMC*, Vol. 53, No. 4, 891–899, Nov. 2011.
6. Hansen, T. B. and A. D. Yaghjian, "Planar near-field scanning in the time domain, Part 2: Sampling theorems and computation schemes," *IEEE Trans. Antennas Propagat.*, Vol. 42, No. 9, 1280–1291, 1994.

7. Serhir, M., P. Besnier, and M. Drissi, "An accurate equivalent behavioural model of antenna radiation using a mode-matching technique based on spherical near field measurements," *IEEE Trans. on Ant. Prop.*, Vol. 56, No. 1, 48–57, Jan. 2008.
8. Las-Heras, F. and T. K. Sarkar, "A direct optimization approach for source reconstruction and NF-FF transformation using amplitude-only data," *IEEE Trans. Ant. Prop.*, Vol. 50, No. 4, 500–510, Apr. 2002.
9. Serhir, M., J. M. Geffrin, A. Litman, and P. Besnier, "Aperture antenna modeling by a finite number of elemental dipoles from spherical field measurements," *IEEE Trans. on Ant. Prop.*, Vol. 58, No. 4, 1260–1268, Apr. 2010.
10. "Information technology equipment, radiated emission tests," International Standard IEC/EN55022, 2007.
11. "Electromagnetic compatibility (EMC) radiated immunity tests — Part 4-3: Testing and measurement techniques — Radiated, radio-frequency, electromagnetic field immunity test," Internation Standard IEC/EN 61000-4-3, 2007.
12. Capozzoli, A., C. Curcio, and A. Liseno, "Experimental field reconstruction of incoherent sources," *Progress In Electromagnetics Research B*, Vol. 47, 219–239, 2013.
13. Laurin, J.-J., Z. Ouardhiri, and J. Colinas, "Near-field imaging of radiated emission sources on printed-circuit boards," *2001 IEEE Int. Symp. on Electromagnetic Compatibility (EMC) Digest*, Vol. 1, 368–373, Montréal, QC, Aug. 13–17, 2001.
14. Deschrijver, D., F. Vanhee, D. Pissoort, and T. Dhaene, "Automated near-field scanning algorithm for the EMC analysis of electronic devices," *IEEE Trans. EMC*, Vol. 54, No. 3, 502–510, Jun. 2012.
15. Liu, Y., B. Ravelo, and P. Fernandez-Lopez, "Modeling of magnetic near-field radiated by electronic devices disturbed by complex transient signals," *Applied Physics Research (APR)*, Vol. 4, No. 1, 3–18, Feb. 2012.
16. Baudry, D., C. Arcambal, A. Louis, B. Mazari, and P. Eudeline, "Applications of the near-field techniques in EMC investigations," *IEEE Trans. Electromagnetic Compatibility*, Vol. 49, No. 3, 485–493, Aug. 2007.
17. Tong, X., D. W. P. Thomas, A. Nothofer, P. Sewell, and C. Christopoulos, "Modelling electromagnetic emissions from printed circuit boards in closed environments using equivalent dipoles," *IEEE Trans. Electromagn. Compat.*, Vol. 52, No. 2, 462–470, 2010.
18. "CST Studio Suite," (2013 CST Computer Simulation Technology AG.), http://www.cst.com-/Content/Products/CST_S2/Overview.aspx, Accessed 2014.
19. "EMPro 3D EM Simulation Software," (Agilent Technologies), http://www.home.agilent.com-/en/pc-1297143/empro-3d-em-simulation-software, Accessed 2013.
20. "Electromagnetics, Circuit & Systems Solutions," (ANSYS Inc.), http://www.ansys.com-/Products/Simulation+Technology/Electromagnetics, Accessed 2013.
21. "EMC Studio," (EMCoS Ltd.), http://www.emcos.com/EMC, Accessed 2014.
22. "Advanced EMC Solutions — FEKO Applications — EMC Analysis," (Advanced EMC Solutions, Inc.), https://www.feko.info/product-detail/overview-of-feko, Accessed 2013.
23. Barrière, P. A., J. J. Laurin, and Y. Goussard, "Mapping of equivalent currents on high-speed digital printed circuit boards based on near-field measurements," *IEEE Trans. Electromagnetic Compatibility*, Vol. 51, No. 3, 649–658, Aug. 2009.
24. Aunchaleevarapan, K., K. Paithoonwatanakij, W. Khan-ngern, and S. Nitta, "Novel method for predicting PCB configurations for near-field and far-field radiated EMI using a neural network," *IEICE Trans. Commun.*, Vol. E86-B, No. 4, 1364–1376, Apr. 2003.
25. Reinhold, C., C. Hangmann, T. Mager, C. Hedayat, and U. Hilleringmann, "Plane wave spectrum expansion from near-field measurements on no-planar lattices," *Proc. 5th Int. Conf. on electromagnetic Near-field Characterization and Imaging (ICONIC) 2011*, 1–4, Rouen, France, Nov. 30–Dec. 2, 2011.
26. Ravelo, B., Y. Liu, and J. Ben Hadj Slama, "Time-domain planar near-field/near-field transform with PWS operations," *Eur. Phys. J. Appl. Phys.*, Vol. 53, No. 1 (30701), 1–8, 2011.
27. Balanis, C. A., *Antenna Theory: Analysis and Design*, 3rd edition, Wiley, New York, 2005.